Astronomy & Astrophysics manuscript no. output
March 6, 2023

Cross-calibration of *ASIM*/HED, Konus-*Wind*, and *Fermi*/GBM instruments using simultaneously detected Gamma-Ray Bursts

March 6, 2023

ABSTRACT

Context. The analysis of a sample of gamma-ray bursts (GRBs) jointly detected by various instruments allows to understand the systematics in the GRB spectral parameters and energetics, which is required when one wants to use the sample of GRBs detected by diverse instruments, e.g., for the population studies.
Aims. The goal of this paper is to present relative spectral cross-calibration of *ASIM*/HED (HED) detector response with Konus-*Wind* (KW) and *Fermi*/GBM (GBM) responses using the simultaneously observed GRBs as calibration sources.
Methods. Using Xspec, we fitted **xx** spectra of **xx** GRBs, simultaneously detected by HED and at least one of the two other instruments, with two phenomenological models: the Band function and an exponentially cut-off power-law.
Results. Based on the joint spectral fits, we found that . . . (some quantitative results).
Conclusions. The joint fits of HED spectra with KW or GBM spectral data provide consistent and better constraints on the peak energies/high-energy indices β. The joint fits of KW and GBM spectral data can enhance constraints on the high-energy photon index β. The energy fluxes obtained from the KW and GBM spectral data are in agreement. The HED fluxes are systematically higher/lower/in agreement with the KW and GBM ones.

Key words. Stars: Gamma-ray burst: general – Methods: observational – Methods: statistical – Techniques: spectroscopic – Instrumentation: spectrographs – Astronomical databases: Miscellaneous – Methods: data analysis

1. Introduction

The precise measurements of the gamma-ray burst (GRB) prompt emission spectra are crucial for understanding their spectral properties and energetics, which, in turn, allows the modeling of their central engines and emission mechanisms. Using the data from distinct instruments in the same study may significantly enlarge the burst sample improving the statistics. For example, for the GRBs with measured redshifts, using the joint samples (hereafter "joint" stands for the simultaneous use of the data collected by different instruments) may provide more **precise/robust/reliable?** parameter estimates for the correlations between the rest-frame spectral parameters and energetics; the luminosity function and the GRB formation rate. However, using joint samples for the population studies requires the relative calibration of detector responses to be in agreement.

The KW response was on-ground calibrated using a set of radioactive sources and is routinely in-flight calibrated using the 1460 keV line of ^{40}K and the 511 keV e^+e^- annihilation line in the multichannel spectra. The GBM response was calibrated on-ground using a set of radioactive sources and the BESSY synchrotron radiation facility. The GBM in-flight calibration is performed using the fits to background lines (e.g., 511 keV). **The HED response . . .** More details and references on these instruments will be provided in Section 2. The interested reader can find the description of all key missions detecting GRBs in Tsvetkova et al. (2022). We carried out the cross-calibration of the energy responses for KW, GBM, and HED, using simultaneously observed GRBs that we report in this paper.

The paper is organized as follows. In Section 2, we detail the KW, GBM, and HED detectors. In Section 3, we delineate the GRB sample used for cross-calibration, describe the methodology of data analysis, and present the results. We discuss and summarize the results in Section 4. The quoted errors in this work are at the **68%** confidence level, unless otherwise stated.

2. Instrumentation

2.1. Konus-Wind

KW is a gamma-ray spectrometer designed to study temporal and spectral characteristics of gamma-ray bursts, solar flares (SFs), SGR bursts, and other transient phenomena over a wide energy range from 13 keV to 10 MeV, nominally (i.e., at launch). It consists of two identical omnidirectional NaI(Tl) detectors, thallium activated with sodium iodide crystals 7.5 cm thick and 12.5 cm in diameter, mounted on opposite faces of the rotationally stabilized *Wind* spacecraft. One detector (S1) points toward the south ecliptic pole, thereby observing the south ecliptic hemisphere; while the other (S2) observes the north ecliptic hemisphere. Each detector has an effective area of ~80–160 cm^2, depending on the photon energy and incident angle. In interplanetary space far outside the Earth's magnetosphere, KW has the advantages over Earth-orbiting GRB monitors of continuous coverage, uninterrupted by Earth

occultation, and a steady background, undistorted by passages through the Earth's trapped radiation, and subject only to occasional solar particle events. The Wind distance from Earth as a function of time is presented in Pal'shin et al. (2013); it ranges up to 7 lt-s.

The instrument has two operational modes: waiting and triggered. The light curves are recorded in three energy windows: G1 (~13–50 keV, nominally, i.e. at launch), G2 (~50–200 keV), and G3 (~200–760 keV) with the time resolution varying from 2 ms to 256 ms in the triggered mode and 2.944 s in the waiting mode. A standard KW dead time (DT) correction procedure is applied to all light curves (with a DT of a few microseconds). When the count rate in the G2 window exceeds a $\sim 9\sigma$ threshold above the background on one of two fixed timescales, 1 s or 140 ms, the instrument switches into the triggered mode, for which the waiting-mode data are also available up to T_0 + 250 s. Spectral measurements are carried out, starting from the trigger time T_0, in two overlapping energy intervals, PHA1 (13–760 keV) and PHA2 (160 keV–10 MeV), with 64 spectra being recorded for each interval over a 63-channel, pseudo-logarithmic, energy scale.

The latest version of the DRM, which is a function only of the burst angle relative to the instrument axis, contains responses calculated for 264 photon energies between 5 keV and 30 MeV on a quasi-logarithmic scale for incident angles from 0°to 100°with a step of 5°. The detailed description of the instrument response calculation is presented in Terekhov et al. (1998). The gain of the detectors has slowly decreased during the long period of operation. The energy scale is calibrated in flight using the 1460 keV line of ^{40}K and the 511 keV e^+ e^- annihilation line in the multichannel spectra. The gauge factor during 2005–2019 varies in the ranges 1.7–2.1 for S1 and 1.5–1.7 for S2. Therefore, the spectral band in the waiting mode ranges from ~**20(17) keV** to **1500(1250) keV** for S1(S2) detectors during the time interval under consideration. A more detailed discussion of the KW instrumental issues can be found in Tsvetkova et al. (2021, 2017); Svinkin et al. (2016).

KW has triggered ~ 4800 times on a variety of transient events, including ~ 3140 GRBs, up to 2018 December. Thus KW has been detecting triggered GRBs at a rate of ≈ 130 events per year. About 27000 events, including ~3200 GRBs, were found in the KW waiting-mode data during the same time interval. The KW databases of short bursts along with their IPN localization maps, GRBs with z, SGRs, and SFs can be found at the KW web page[1].

2.2. Fermi/GBM

The *Fermi* Gamma-ray Space Telescope, dedicated to study transient gamma-ray sources, was launched in June 2008. It harbors two scientific instruments: the Gamma-ray Burst Monitor (GBM; Meegan et al. 2009) and the Large Area Telescope (LAT; Atwood et al. 2009). The LAT is sensitive in the energy range from 30 MeV to 300 GeV, while the GBM, which direct experimental objective was to identify and study GRBs, covers the energy range from 8 keV to 40 MeV, extending the energy range over which bursts are observed from the LAT energy range downward to the hard X-ray range. The GBM observes the whole sky that is not occulted by the Earth (> 8 sr). GBM is composed of twelve NaI(Tl) detectors and two bismuth germanate (BGO) scintillation detectors. With a thickness of 1.27 cm and a diameter of 12.7 cm, the NaI crystals cover an energy range 8 keV–1 MeV. They are oriented around the spacecraft, three at each of the four corners in a way that the position of the GRB can be determined from the relative count rates seen in the individual detectors. The two BGO crystals have a diameter and thickness of 12.7 cm, covering an energy range of 200 keV–40 MeV, and are located on opposite sides of the spacecraft so that at least one is always illuminated from any direction.

A detailed detector response model has been developed based on Geant4 simulations and confirmed by extensive ground testing, which included the calibration with radioactive sources (from 14.4 keV to 4.4 MeV), the low-energy calibration of the NaI detectors performed at the synchrotron radiation facility BESSY, and the high-energy calibration of the BGO detectors carried out at the SLAC National Accelerator Laboratory, in order to determine the response as a function of orientation (Hoover et al. 2008; Bissaldi et al. 2009). In flight, fits to background lines (e.g., 511 keV) over time show a stable gain and energy resolution in all the GBM detectors and electronics, with lines typically within 1% of their expected position (Wilson-Hodge et al. 2011). The GBM detectors and their calibration are described in more details in Meegan et al. (2009); Bissaldi et al. (2009); Paciesas et al. (2012).

Add trigger statistics.

2.3. ASIM/HED

Add text.

3. Analysis and results

3.1. Analysis methodology

We extracted a set of **xx** GRBs which were simultaneously detected by HED and at least three instruments in the triggered mode. To select the time intervals for spectral analysis, we plotted the KW (G1–G3, ~20–1200 keV), HED **(xx–xx keV)**, GBM (8 keV–1 MeV and 200 keV–40 MeV) light curves with the boundaries of KW spectra marked on them. First, we shift the light curves to take into account the light propagation time between the spacecrafts. Then, since the ISS clock used by HED are imprecise, we cross-correlate the HED and KW light curves. **Mention the GBM and KW cross-correlation.** Figure 1 shows an example of the light curves of the three instruments. Since the time resolution of the first four KW spectra is fixed to 64 ms, we choose the intervals for the spectral analyses according to the KW spectrum accumulation times.

The general information about the burst sample is presented in Table 1. The first two columns contain the GRB name as reported in the Gamma-ray Burst Coordinates Network circulars[2] and KW geocentric trigger time (the time corrected for the burst front

[1] http://www.ioffe.ru/LEA/

[2] http://gcn.gsfc.nasa.gov/gcn3_archive.html

propagation from *Wind* to the Earth center). The next two columns provide the HED and GBM burst IDs. The next three columns provide the GRB localization along with the reference and the two rightmost columns contain the light propagation times (ToF; time of flight).

The KW data are processed using standard KW analysis tools, which convert the spectral data collected on-board from the internal format to two calibrated pulse height amplitude PHA II files in FITS format suitable for spectral analysis. The dead-time correction has been applied. For the given incident angle, two DRMs corresponding to each PHA were calculated by linear interpolation of the DRMs for the nearest angles. Since the spacecraft is situated at the Lagrange point L1, the background is stable in time on the timescale of GRB. Thus, the background level was approximated with a constant over a ∼**100–200 s** long quiescence interval after the burst.

We retrieved the GBM time-tagged event (TTE) files and response matrices from the Fermi Science Support Center repository[3]. To estimate the background level, we selected two time intervals: before and after the source time interval according to the GBM public GRB burst catalogue[4] For spectral analysis, we used the same detectors as selected in the **xx-files**. The GBM fits-files containing the source and background spectra were prepared using the Fermi GBM Data Tools[5]. **We also checked the selected detectors for blockage by the parts of the spacecraft.** For every spectrum, we used the BGO detector with the smaller incident angle. While performing spectral analysis, we ignored **xx channels** of the NaI spectra and **xx channels** of the BGO spectra.

Description of the HED data reduction procedure.

Using Xspec Arnaud (1996), each spectrum was fitted by two empirical spectral models, both normalized at 100 keV. The first model is the Band function (hereafter BAND; Band et al. 1993):

$$f(E) \propto \begin{cases} E^{\alpha} \exp\left(-\frac{E(2+\alpha)}{E_{\rm p}}\right), & E < (\alpha-\beta)\frac{E_{\rm p}}{2+\alpha} \\ E^{\beta}\left[(\alpha-\beta)\frac{E_{\rm p}}{(2+\alpha)}\right]^{(\alpha-\beta)} \exp(\beta-\alpha), & E \geq (\alpha-\beta)\frac{E_{\rm p}}{2+\alpha}, \end{cases} \quad (1)$$

where α is the low-energy photon index, β is the high-energy photon index, and $E_{\rm p}$ is the maximum of νF_{ν} spectrum.

The second spectral model is an exponentially cutoff power-law (CPL):

$$f(E) \propto E^{\alpha} \exp\left(-\frac{E(2+\alpha)}{E_{\rm p}}\right). \quad (2)$$

Mention the fit statistics. Try CSTAT and PGSTAT too.

When fitting, (1) the KW PHA1 channels above ∼400 keV were excluded as they intercept with the initial channels of PHA2; (2) **the HED channels below 400 keV were ignored;** (3) **regarding to GBM, we used the 250–30000 keV energy range for the BGO detectors and the 9–900 keV band for the NaI detectors.**

When possible, we fitted a set of different combinations of spectral data from the three gamma-telescopes, namely, KW+HED+GBM, KW+GBM, KW+HED, HED+GBM, and KW, GBM, HED (the data from single instruments) to allow a comparison with joint fits. The responses were multiplied by a constant normalization factor to take into account the systematic effective area uncertainties in the response matrices of each instrument. For joint KW+HED+GBM, KW+HED, KW+GBM fits, the normalization factor of the **KW** data was fixed to unity, while the normalization factors of the **HED** and the GBM spectra were left free. The normalization factor between the GBM NaI When fitting HED+GBM, the normalization factor of the HED data was fixed to unity, while the normalization factors of the GBM NaI and BGO detectors were free parameters. When fitting the GBM only data, the normalization factors for all but one detectors were left free.

3.2. GRB 201227A

GRB 201227A triggered the S1 KW detector, the incident angle to which is 25.9. We used the data from three GBM detectors, namely n4 (triggered), n8 (triggered), and b0 (The Sun is visible to this detector), for which the incident angles are about 45°, 68°, and 73°. We extracted the spectral files and approximated the background using `GBM Data Tools`[6]. Taking into account the light propagation time("time of flight", hereafter, ToF) between *Wind* and *Fermi* and the difference in the KW and GBM trigger times, the GBM data was shifted to $T_{0\rm GBM}$ + 2 ms. **Description of ASIM time shifts, cross-correlation and uncertainties of the ISS clock.**

4. Discussion and conclusions

[3] `https://heasarc.gsfc.nasa.gov/FTP/fermi/data/gbm/bursts/`
[4] `https://heasarc.gsfc.nasa.gov/W3Browse/fermi/fermigbrst.html`
[5] `https://fermi.gsfc.nasa.gov/ssc/data/analysis/gbm/gbm_data_tools/gdt-docs/`
[6] `https://fermi.gsfc.nasa.gov/ssc/data/analysis/gbm/gbm_data_tools/gdt-docs/index.html`

Table 1. General Information

Burst name	KW Geocentric time (s)	HED Trigger #	GBM Trigger #	RA (deg)	Dec (deg)	Refs	$\mathrm{ToF}_{\mathrm{Wind-ISS}}$	$\mathrm{ToF}_{\mathrm{Fermi-ISS}}$

Table 2. Spectrum accumulation times

Burst name	Spectrum	T_{start}[1] (s)	T_{stop} (s)	Sample	GBM detectors	α	β	E_{p}	F	n_{HED}	n_{NaI}[2]	n_{BGO}

[1] The spectrum start and end times are given in UT.
[2] GBM detector.

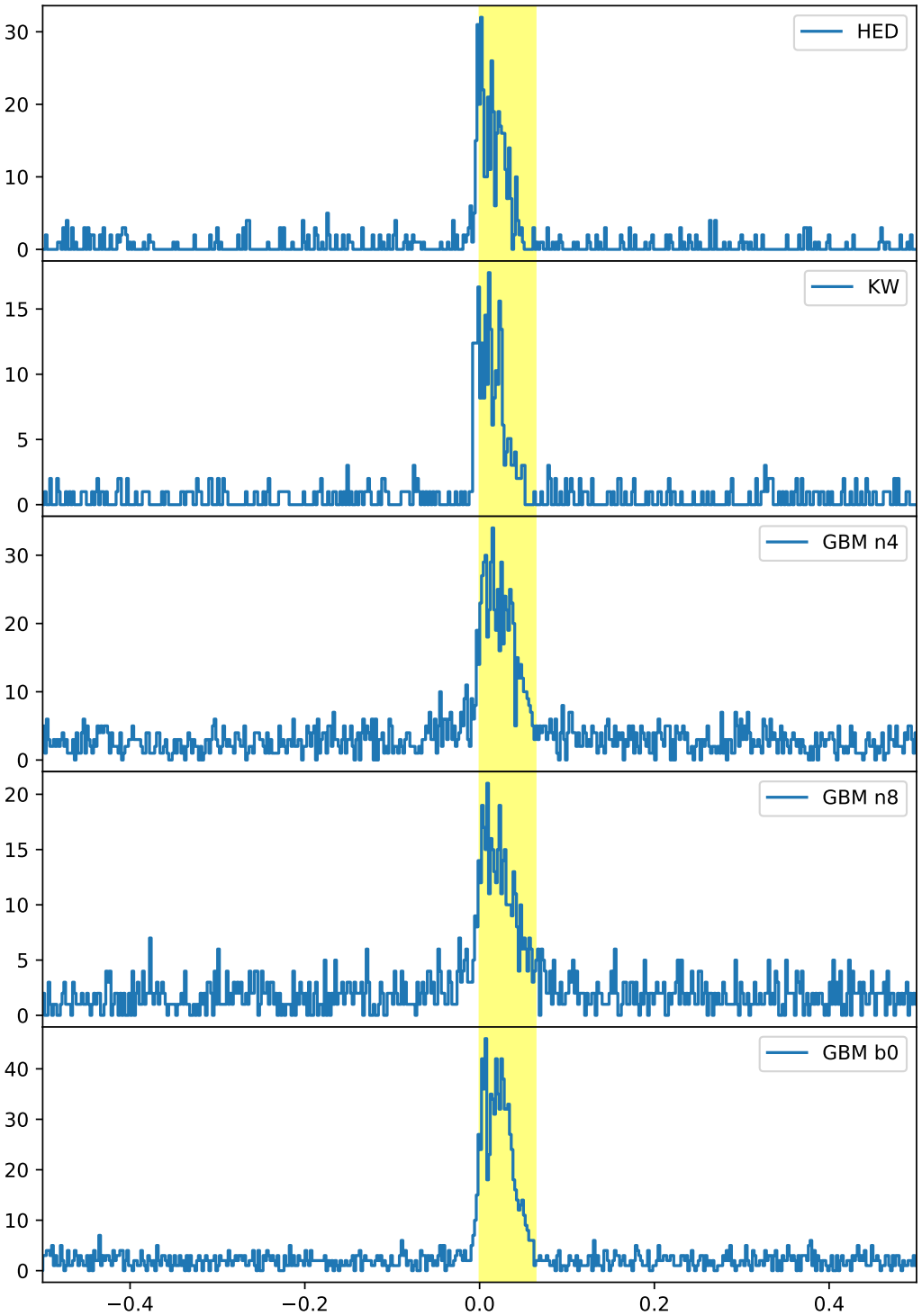

Fig. 1. Example of KW, BAT, and GBM light curves. The HED and KW light curves are cross-correlated and all light curves are corrected to the light propagation times between the spacecrafts. The KW trigger mode light curve record starts -0.512 s before the trigger.

Fig. 2. Plots of spectral fits for HED, KW, and GBM along with the residuals(from left to right).

References

K. A. Arnaud. XSPEC: The First Ten Years. In George H. Jacoby and Jeannette Barnes, editors, *Astronomical Data Analysis Software and Systems V*, volume 101 of *Astronomical Society of the Pacific Conference Series*, page 17, January 1996.

W. B. Atwood, A. A. Abdo, M. Ackermann, W. Althouse, B. Anderson, M. Axelsson, L. Baldini, J. Ballet, D. L. Band, G. Barbiellini, J. Bartelt, D. Bastieri, B. M. Baughman, K. Bechtol, D. Bédérède, F. Bellardi, R. Bellazzini, B. Berenji, G. F. Bignami, D. Bisello, E. Bissaldi, R. D. Blandford, E. D. Bloom, J. R. Bogart, E. Bonamente, J. Bonnell, A. W. Borgland, A. Bouvier, J. Bregeon, A. Brez, M. Brigida, P. Bruel, T. H. Burnett, G. Busetto, G. A. Caliandro, R. A. Cameron, P. A. Caraveo, S. Carius, P. Carlson, J. M. Casandjian, E. Cavazzuti, M. Ceccanti, C. Cecchi, E. Charles, A. Chekhtman, C. C. Cheung, J. Chiang, R. Chipaux, A. N. Cillis, S. Ciprini, R. Claus, J. Cohen-Tanugi, S. Condamoor, J. Conrad, R. Corbet, L. Corucci, L. Costamante, S. Cutini, D. S. Davis, D. Decotigny, M. DeKlotz, C. D. Dermer, A. de Angelis, S. W. Digel, E. do Couto e Silva, P. S. Drell, R. Dubois, D. Dumora, Y. Edmonds, D. Fabiani, C. Farnier, C. Favuzzi, D. L. Flath, P. Fleury, W. B. Focke, S. Funk, P. Fusco, F. Gargano, D. Gasparrini, N. Gehrels, F. X. Gentit, S. Germani, B. Giebels, N. Giglietto, P. Giommi, F. Giordano, T. Glanzman, G. Godfrey, I. A. Grenier, M. H. Grondin, J. E. Grove, L. Guillemot, S. Guiriec, G. Haller, A. K. Harding, P. A. Hart, E. Hays, S. E. Healey, M. Hirayama, L. Hjalmarsdotter, R. Horn, R. E. Hughes, G. Jóhannesson, G. Johansson, A. S. Johnson, R. P. Johnson, T. J. Johnson, W. N. Johnson, T. Kamae, H. Katagiri, J. Kataoka, A. Kavelaars, N. Kawai, H. Kelly, M. Kerr, W. Klamra, J. Knödlseder, M. L. Kocian, N. Komin, F. Kuehn, M. Kuss, D. Landriu, L. Latronico, B. Lee, S. H. Lee, M. Lemoine-Goumard, A. M. Lionetto, F. Longo, F. Loparco, B. Lott, M. N. Lovellette, P. Lubrano, G. M. Madejski, A. Makeev, B. Marangelli, M. M. Massai, M. N. Mazziotta, J. E. McEnery, N. Menon, C. Meurer, P. F. Michelson, M. Minuti, N. Mirizzi, W. Mitthumsiri, T. Mizuno, A. A. Moiseev, C. Monte, M. E. Monzani, E. Moretti, A. Morselli, I. V. Moskalenko, S. Murgia, T. Nakamori, S. Nishino, P. L. Nolan, J. P. Norris, E. Nuss, M. Ohno, T. Ohsugi, N. Omodei, E. Orlando, J. F. Ormes, A. Paccagnella, D. Paneque, J. H. Panetta, D. Parent, M. Pearce, M. Pepe, A. Perazzo, M. Pesce-Rollins, P. Picozza, L. Pieri, M. Pinchera, F. Piron, T. A. Porter, L. Poupard, S. Rainò, R. Rando, E. Rapposelli, M. Razzano, A. Reimer, O. Reimer, T. Reposeur, L. C. Reyes, S. Ritz, L. S. Rochester, A. Y. Rodriguez, R. W. Romani, M. Roth, J. J. Russell, F. Ryde, S. Sabatini, H. F. W. Sadrozinski, D. Sanchez, A. Sander, L. Sapozhnikov, P. M. Saz Parkinson, J. D. Scargle, T. L. Schalk, G. Scolieri, C. Sgrò, G. H. Share, M. Shaw, T. Shimokawabe, C. Shrader, A. Sierpowska-Bartosik, E. J. Siskind, D. A. Smith, P. D. Smith, G. Spandre, P. Spinelli, J. L. Starck, T. E. Stephens, M. S. Strickman, A. W. Strong, D. J. Suson, H. Tajima, H. Takahashi, T. Takahashi, T. Tanaka, A. Tenze, S. Tether, J. B. Thayer, J. G. Thayer, D. J. Thompson, L. Tibaldo, O. Tibolla, D. F. Torres, G. Tosti, A. Tramacere, M. Turri, T. L. Usher, N. Vilchez, V. Vitale, P. Wang, K. Watters, B. L. Winer, K. S. Wood, T. Ylinen, and M. Ziegler. The Large Area Telescope on the Fermi Gamma-Ray Space Telescope Mission. *ApJ*, 697(2):1071–1102, June 2009. .

D. Band, J. Matteson, L. Ford, B. Schaefer, D. Palmer, B. Teegarden, T. Cline, M. Briggs, W. Paciesas, G. Pendleton, G. Fishman, C. Kouveliotou, C. Meegan, R. Wilson, and P. Lestrade. BATSE observations of gamma-ray burst spectra. I - Spectral diversity. *ApJ*, 413:281–292, August 1993. .

E. Bissaldi, A. von Kienlin, G. Lichti, H. Steinle, P. N. Bhat, M. S. Briggs, G. J. Fishman, A. S. Hoover, R. M. Kippen, M. Krumrey, M. Gerlach, V. Connaughton, R. Diehl, J. Greiner, A. J. van der Horst, C. Kouveliotou, S. McBreen, C. A. Meegan, W. S. Paciesas, R. D. Preece, and C. A. Wilson-Hodge. Ground-based calibration and characterization of the Fermi gamma-ray burst monitor detectors. *Experimental Astronomy*, 24(1-3):47–88, May 2009. .

A. S. Hoover, R. M. Kippen, M. S. Wallace, G. N. Pendleton, G. J. Fishman, C. A. Meegan, C. Kouveliotou, C. A. Wilson-Hodge, E. Bissaldi, R. Diehl, J. Greiner, G. G. Lichti, A. von Kienlin, H. Steinle, P. N. Bhat, M. S. Briggs, V. Connaughton, W. S. Paciesas, and R. D. Preece. GLAST Burst Monitor Instrument Simulation and Modeling. In M. Galassi, David Palmer, and Ed Fenimore, editors, *Gamma-ray Bursts 2007*, volume 1000 of *American Institute of Physics Conference Series*, pages 565–568, May 2008. .

Charles Meegan, Giselher Lichti, P. N. Bhat, Elisabetta Bissaldi, Michael S. Briggs, Valerie Connaughton, Roland Diehl, Gerald Fishman, Jochen Greiner, Andrew S. Hoover, Alexander J. van der Horst, Andreas von Kienlin, R. Marc Kippen, Chryssa Kouveliotou, Sheila McBreen, W. S. Paciesas, Robert Preece, Helmut Steinle, Mark S. Wallace, Robert B. Wilson, and Colleen Wilson-Hodge. The Fermi Gamma-ray Burst Monitor. *ApJ*, 702(1):791–804, September 2009. .

William S. Paciesas, Charles A. Meegan, Andreas von Kienlin, P. N. Bhat, Elisabetta Bissaldi, Michael S. Briggs, J. Michael Burgess, Vandiver Chaplin, Valerie Connaughton, Roland Diehl, Gerald J. Fishman, Gerard Fitzpatrick, Suzanne Foley, Melissa Gibby, Misty Giles, Adam Goldstein, Jochen Greiner, David Gruber, Sylvain Guiriec, Alexander J. van der Horst, R. Marc Kippen, Chryssa Kouveliotou, Giselher Lichti, Lin Lin, Sheila McBreen, Robert D. Preece, Arne Rau, Dave Tierney, and Colleen Wilson-Hodge. The Fermi GBM Gamma-Ray Burst Catalog: The First Two Years. *ApJS*, 199(1):18, March 2012. .

V. D. Pal'shin, K. Hurley, D. S. Svinkin, R. L. Aptekar, S. V. Golenetskii, D. D. Frederiks, E. P. Mazets, P. P. Oleynik, M. V. Ulanov, T. Cline, I. G. Mitrofanov, D. V. Golovin, A. S. Kozyrev, M. L. Litvak, A. B. Sanin, W. Boynton, C. Fellows, K. Harshman, J. Trombka, T. McClanahan, R. Starr, J. Goldsten, R. Gold, A. Rau, A. von Kienlin, V. Savchenko, D. M. Smith, W. Hajdas, S. D. Barthelmy, J. Cummings, N. Gehrels, H. Krimm, D. Palmer, K. Yamaoka, M. Ohno, Y. Fukazawa, Y. Hanabata, T. Takahashi, M. Tashiro, Y. Terada, T. Murakami, K. Makishima, M. S. Briggs, R. M. Kippen, C. Kouveliotou, C. Meegan, G. Fishman, V. Connaughton, M. Boër, C. Guidorzi, F. Frontera, E. Montanari, F. Rossi, M. Feroci, L. Amati, L. Nicastro, M. Orlandini, E. Del Monte, E. Costa, I. Donnarumma, Y. Evangelista, I. Lapshov, F. Lazzarotto, L. Pacciani, M. Rapisarda, P. Soffitta, G. Di Cocco, F. Fuschino, M. Galli, C. Labanti, M. Marisaldi, J. L. Atteia, R. Vanderspek, and G. Ricker. Interplanetary Network Localizations of Konus Short Gamma-Ray Bursts. *ApJS*, 207(2):38, August 2013. .

D. S. Svinkin, D. D. Frederiks, R. L. Aptekar, S. V. Golenetskii, V. D. Pal'shin, P. P. Oleynik, A. E. Tsvetkova, M. V. Ulanov, T. L. Cline, and K. Hurley. The Second Konus-Wind Catalog of Short Gamma-Ray Bursts. *ApJS*, 224:10, May 2016. .

M. M. Terekhov, R. L. Aptekar, D. D. Frederiks, S. V. Golenetskii, V. N. Il'Inskii, and E. P. Mazets. The Konus-Wind and Konus-A instrument response functions and the spectral deconvolution procedure. In C. A. Meegan, R. D. Preece, and T. M. Koshut, editors, *Gamma-Ray Bursts, 4th Hunstville Symposium*, volume 428 of *American Institute of Physics Conference Series*, pages 894–898, May 1998. .

A. Tsvetkova, D. Frederiks, S. Golenetskii, A. Lysenko, P. Oleynik, V. Pal'shin, D. Svinkin, M. Ulanov, T. Cline, K. Hurley, and R. Aptekar. The Konus-Wind Catalog of Gamma-Ray Bursts with Known Redshifts. I. Bursts Detected in the Triggered Mode. *ApJ*, 850:161, December 2017. .

Anastasia Tsvetkova, Dmitry Frederiks, Dmitry Svinkin, Rafail Aptekar, Thomas L. Cline, Sergei Golenetskii, Kevin Hurley, Alexandra Lysenko, Anna Ridnaia, and Mikhail Ulanov. The Konus-Wind Catalog of Gamma-Ray Bursts with Known Redshifts. II. Waiting-Mode Bursts Simultaneously Detected by Swift/BAT. *ApJ*, 908(1):83, February 2021. .

Anastasia Tsvetkova, Dmitry Svinkin, Sergey Karpov, and Dmitry Frederiks. Key Space and Ground Facilities in GRB Science. *Universe*, 8(7):373, July 2022. .

Colleen A. Wilson-Hodge, Michael L. Cherry, Gary L. Case, Wayne H. Baumgartner, Elif Beklen, P. Narayana Bhat, Michael S. Briggs, Ascension Camero-Arranz, Vandiver Chaplin, Valerie Connaughton, Mark H. Finger, Neil Gehrels, Jochen Greiner, Keith Jahoda, Peter Jenke, R. Marc Kippen, Chryssa Kouveliotou, Hans A. Krimm, Erik Kuulkers, Niels Lund, Charles A. Meegan, Lorenzo Natalucci, William S. Paciesas, Robert Preece, James C. Rodi, Nikolai Shaposhnikov, Gerald K. Skinner, Doug Swartz, Andreas von Kienlin, Roland Diehl, and Xiao-Ling Zhang. When a Standard Candle Flickers. *ApJ*, 727(2):L40, February 2011. .